Indoor dual polarised radio channel characterization in the 54 GHz and 70 GHz bands

Indoor Dual Polarised Radio Channel Characterization in the 54 GHz and 70 GHz bands

Xavier Z. Raimundo, Sana Salous, Adnan A. Cheema

School of Engineering and Computing Sciences, Durham University, South Road, Durham, DH1 3LE, United Kingdom

Abstract: In this paper, results of wideband dual polarised measurements conducted in indoor environments including office, factory, corridor and computer foyer, using state the art 2 by 2 multiple input multiple output (MIMO) Frequency Modulated Continuous Wave (FMCW) based channel sounder, are presented. The measurements were performed in two frequency bands with 6 GHz bandwidth, centred at 54 GHz and 70 GHz, with directional steerable ~20 dBi (18 degrees beamwidth) horn antennas. Using twists at the transmitter and at the receiver simultaneous co-polar and cross-polar measurements were performed to quantify the polarization effects on channel parameters such as angular spread, delay spread and path loss. The results show that the co-polarized radio links experienced lower angular spread and delay spread compared with the cross polarized links. For co-polarized links, the estimated synthesized omnidirectional path loss exponent was found to be in the range of 1.5-2 (close-in model) and 0.9-1.9 (log-distance model) in the respective environments. In individual scenarios, the median cross polarization ratio was found to be within 11.7-14.4 dB and 7.5-17.6 dB at 54 GHz and 70 GHz, respectively.

1. Introduction

The increasing demand for higher data traffic in wireless communication networks and the lack of available wide bandwidths in the sub 10 GHz spectrum band has prompted the research community, industry and the regulators to consider alternative bands. The millimetre-wave band up-to 100 GHz, with large contiguous unallocated sections of the spectrum is seen as a possible solution to overcome the spectrum requirements for future wireless networks.

In November 2015 the World Radio-communications Conference, WRC15, identified a number of frequency bands in the 24-86 GHz range (24.25-27.5 GHz, 31.8-33.4 GHz, 37-43.5 GHz, 45.5-50.2 GHz, 50.4-52.6 GHz, 66-76 GHz and 81-86 GHz) as potential candidates for 5G technology with bandwidths ranging from 1.6-10 GHz. The use of (multiple) underutilised wide bandwidths will considerably enhance the throughput of future networks. Although, millimetre wave communication offers the potential of high data rate there are also challenges that need to be addressed some of which are primarily related to the undesired characteristics of the propagation channel in these bands [1, 2]. Millimetre waves suffer predominantly from high propagation loss and susceptibility to shadowing (e.g. blockage by humans or obstacles). It is envisaged that 5G would employ high gain beam steerable antenna arrays to compensate for these impairments. The exploitation of space-time dimensionalities as well as frequency, in order to maximize the coverage and throughput, are the key features in 5G technology. The development of propagation models that fully characterise the spatial and temporal behaviour of the channel in the aforementioned bands is a key for successful development of 5G wireless systems.

A significant amount of indoor channel propagation measurements in the millimetre wave band have been reported in the literature in the unlicensed 60 GHz band [3-9]. Measured scenarios include corridors, offices, conference rooms and hallways for co-polarised links. The reported channel parameters include path loss models [3, 4], shadowing due to human activity [5], small–scale spatial and temporal statistics [6-8], and wall and floor penetration loss [9]. Other reported work within the millimetre wave bands includes: path loss in the 28 GHz and 73 GHz bands detailed in [10] for the aforementioned scenarios, and at 45 GHz [11] in which residential (e.g. living room) and office like environments are considered. Moreover, comparison of the delay spread at 60 GHz and 70 GHz in an office, shopping mall and railway station are presented in [12], and the spatial and temporal statistics at 83 GHz for office like scenarios are discussed in [13]. Amongst, these works only [10] and [11] reported results of co-polar and cross-polar measurements. Therefore, dual polarised measurements across the WRC15 bands, and especially in scenarios such as laboratory, factory or residential environments are seldom reported.

In this paper, results of wideband channel measurements conducted in an office, factory, corridor and computer foyer in the frequency bands 51-57 GHz and 67-73 GHz using the custom designed multiband linear Frequency Modulated Continuous Wave (FMCW or chirp) based channel sounder [4] are presented. The data were analysed with 2 GHz

bandwidth to estimate channel parameters including path loss, angular spread, *r.m.s.* delay spread and cross polar discrimination.

The rest of the paper is organised as follows: section 2 gives an overview of the experimental set-up and the measured scenarios; section 3 outlines the channel parameters to be estimated and presents the corresponding results, with conclusions and recommendations for further work presented in section 4.

2. Measurement Set-up and Scenarios

The measurements were performed using a multiband 2x2 MIMO FMCW channel sounder. In this section a brief summary of the channel sounder is provided and further details regarding its architecture and performance can be found in [4].

The sounder comprises of two dedicated units (the main unit and an RF unit). The main unit consists of a programmable baseband FMCW generator, followed by up-converter sub-units which allows simultaneous independent operation in the frequency bands below 6 GHz bands (0.25 – 1 GHz, 2.2 – 2.9 GHz and 4.4 – 5.9 GHz). To enable the coverage of the WRC15 frequency bands a new programmable Intermediate Frequency (IF) sub-unit that enables the generation of 1.5 GHz bandwidth in the frequency range of 12.25 – 18.25 GHz was designed and implemented to replace the fixed band unit reported in [4]. The IF sub-unit output is fed into the dual channel V–band RF unit which contains two parallel times four frequency multipliers, thus enabling up to 6 GHz bandwidth in the 50-73 GHz frequency range. Details of the up-conveter unit and the performance of the sounder can be found in [4]. To enable 2x2 MIMO measurements the IF output is switched between the two up-converters at the transmitter while at the receiver the IF input is fed simultaneously to the two up-converters for heterodyne detection.

For comparative measurements the frequency bands of 51-57 GHz and 67-73 GHz were measured in the same environment in two runs at similar locations where possible. Horn antennas with typical gain of ~20 dBi, a half power beam-width of ~18° and cross polarization isolation of ~40 dB across the band were used. To perform dual polarised measurements, a polarization twist is used on one channel at the transmitter and one channel at the receiver. Thus, four different transmitter (Tx) and receiver (Rx) polarization links were obtained: vertical-vertical (V-V), vertical-horizontal (V-H), horizontal-horizontal (H-H) and horizontal-vertical (H-V). To estimate the angular variations of the channel parameters, and synthesise an omnidirectional received signal, the RF head at the receiver was mounted on a rotary actuator and rotated in a clockwise direction in steps of 5 degrees to provide full 360-degree azimuthal coverage. The transmitter and receiver units were mounted on an individual four-wheel trolley, for easy mobility as shown in figure 1.

(a) (b)

Fig. 1. *Channel sounding system mounted on trolley (a) transmitter and (b) receiver.*

The measurements were collected with a waveform repetition rate of 1.22 kHz. To aid in the distinction of the different transmit antenna polarisations a four-way switch is used at the transmitter which gives an effective repetition rate of 305 Hz per transmit-receive antenna pair. Data were collected using a 14-bit analogue-to-digital converter sampling at 40 MHz. For each angular rotation, one second of data was recorded. Table 1 provides a summary of the measurement set-up.

A number of scenarios were measured, which include corridor, office, computer foyer, and factory shown in Figure 2. The transmit antenna height was set depending on the ceiling height in the measured environment between 2.2-2.9 metres above ground while the receiver antenna was fixed at 1.6 metres to mimic an average human height. At each location 73 data files were recorded corresponding to the full azimuthal coverage.

Table 1 *Sounder unit set-up parameters*

Parameter	
Frequency range (GHz)	51-57; 67-73
Sweep rate (kHz)	1.22
Data digitisng frequency (MHz)	40
Transmit Power (dBm)	7
Tx/Rx polarization	V-V; V-H; H-V; H-H
Antenna configuration	2x2
Antenna type (gain in dBi)	Standard Horn (20)
Beamwidth (azimuth, elevation)	18.4°; 14.4°
Tx antenna height (m)	2.2-2.9
Rx antenna height (m)	1.6

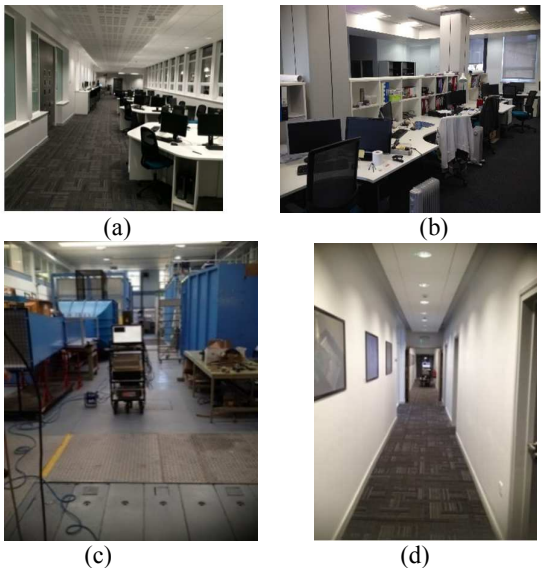

(a) (b) (c) (d)

Fig. 2. *Measured scenarios (a) computer foyer, (b) office, (c) factory, (d) corridor*

The layout of the measurements environment with the transmitter and receiver locations marked as "cross" and "circle" respectively are shown in Figure 3. At the "Tx" the arrow indicates the direction of the main beam while at the "Rx" it indicates the direction of the main beam at rotation angle of 0°. In each scenario the transmitter location was fixed while the receiver unit was moved onto pre-defined locations within the scenario. The inter-distance between consecutive receiver positions varied between 1-3 metres. Table 2 summarizes the minimum and maximum horizontal range between the Tx and Rx.

Table 2 *The Tx-Rx range*

Scenarios	Tx/Rx range (m)
Factory	6 – 29
Corridor	4.4-27
Computer Foyer	6-27
Office	5-16

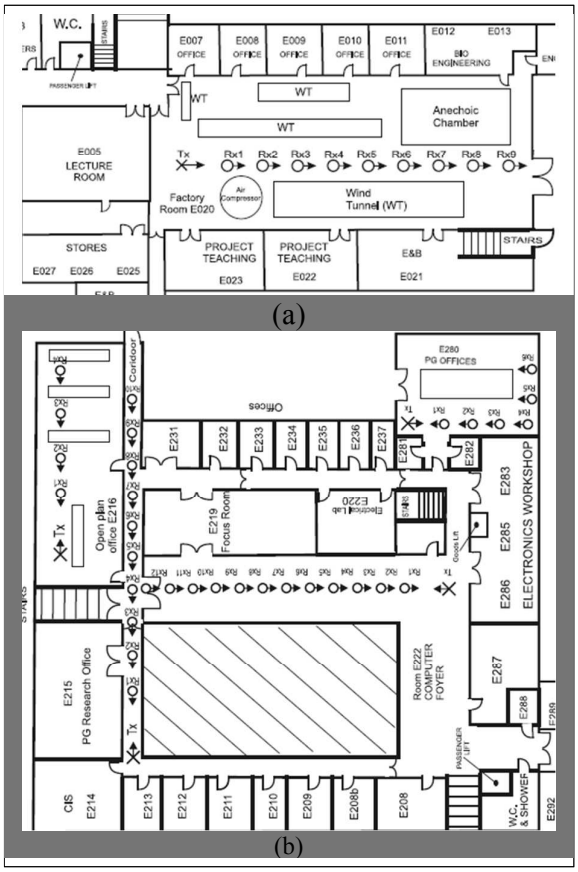

Fig. 3 *Layout of the building floors where the measurements were conducted. (a) for the factory scenario, (b) offices, corridor and computer foyer scenario.*

3. Results and Analyses

Since a frequency modulated continuous wave signal has a linear relationship between time and frequency, the recorded data can be analysed with different time delay resolutions by dividing the sweep duration into a number of sections. In this study the raw data were analysed for 0.5 ns time delay resolution equivalent to 2 GHz bandwidth. Four parameters were estimated in this work: angular spread, delay spread, cross polar discrimination ratio, and path loss. These parameters were estimated from the channel power delay profile (PDP), given in (1), which is the average of the bandlimited channel impulse response $h_k(t_k,\tau)$ for each angle of rotation of the receiver.

$$P(\tau) = \sum_{k=1}^{K} |h_k(t_k,\tau)|^2 / K \quad (1)$$

where "τ" is time delay and "K" is the total number of channel impulse responses obtained in each direction within the one second period of acquisition. Figure 4(a-d) shows an example of the computed power delay profile versus the receiver rotation angle for the four polarisations normalized to the maximum received

signal level over all PDPs in the computer foyer scenario at 54 GHz.

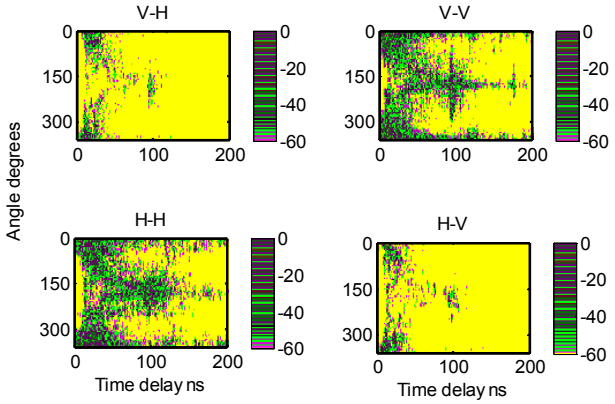

Fig. 4 *Normalized PDP versus azimuth angle of rotation in the computer foyer scenario at 54 GHz*

Strong signal levels can be seen at around 0° and 355° which correspond to the boresight angles where the Rx and Tx antennas were oriented toward each other. Another peak appears at ~180 ° at ~100 ns time delay which corresponds to the reflection from the glass wall at one end of the scenario.

The received power ($P_R(\phi_i)$), at each azimuthal angle, ϕ_i, is given by (2) as the sum of the corresponding noise free power delay profile. Noise samples were excluded from the computation by using a threshold above the corresponding PDP's noise floor. A threshold of four times the computed standard deviation (σ_n) of noise was used. This is based on the assumption that the noise is Gaussian distributed where 95% of the values are within $2\sigma_n$ from the mean [14]. Figure 5 shows the corresponding computed power angle profile (PAP) for each link in Figure 4.

$$P_R(\phi_i) = \sum_{n=1}^{N} P(\tau_n, \phi_i) \quad (2)$$

Due to the limited number of measurement points in each scenario, the data were grouped together into a single co-polarised link (V-V and H-H), and cross-polarised link (V-H and H-V). The statistics of the angular spread, delay spread and path loss model were then estimated for co and cross polarised links.

3.1 Angular Spread

The angular spread of the channel characterizes the directional distribution of the arriving energy. For multiple antenna systems, it can provide an indication of the extent of spatial correlation. In this work, the azimuthal arrival angular spread " ϕ_{rms} " was estimated from the received power angle profile "$P_R(\phi_i)$" using (3).

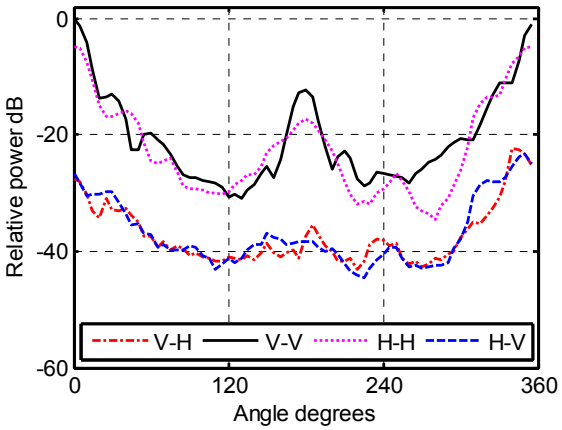

Fig. 5. *Received power as function of rotation angle in the computer foyer scenario at 54 GHz*

$$\phi_{rms} = \sqrt{\frac{\sum_{i=1}^{L} P_R(\emptyset_i)(\emptyset_i - \mu_\emptyset)^2}{\sum_{i=1}^{L} P_R(\emptyset_i)}} \quad (3)$$

where "L" is the total number of angular positions, "ϕ_i" is the corresponding angle, in radian, and "$\mu_\emptyset$" is the mean azimuthal arrival direction given in (4) [15,16].

$$\mu_\emptyset = arg\left(\frac{\sum_{i=1}^{L} P_R(\emptyset_i) e^{i\emptyset_i}}{\sum_{i=1}^{L} P_R(\emptyset_i)}\right) \quad (4)$$

where "*arg*(.)" represents the argument of the expression giving the angle in radians. Taking into account the cyclic nature of the angle, the term $(\emptyset_i - \mu_\emptyset)$ in (3) is constrained within the interval ($-\pi$, π) by wrapping the angle as in [16]: $(\emptyset_i - \mu_\emptyset)$ is replaced by $(\emptyset_i - \mu_\emptyset)$ -2π, when it is greater than π, and by $(\emptyset_i - \mu_\emptyset)$ $+2\pi$ when it is less than $-\pi$.

Figure 6 displays the computed cumulative distribution function (CDF) of the angular spread values for the computer foyer scenario. Table 3 gives the 50% and 90% CDF levels and the corresponding standard deviation $\sigma_{\emptyset_{rms}}$ of the angular spread for the individual scenarios.

The results indicate that the co-polar links exhibits on average a smaller angular spread in comparison with the corresponding cross-polar links. This is because the relative power in the direction of the transmitter is much stronger than in other directions, as seen in figure 5.

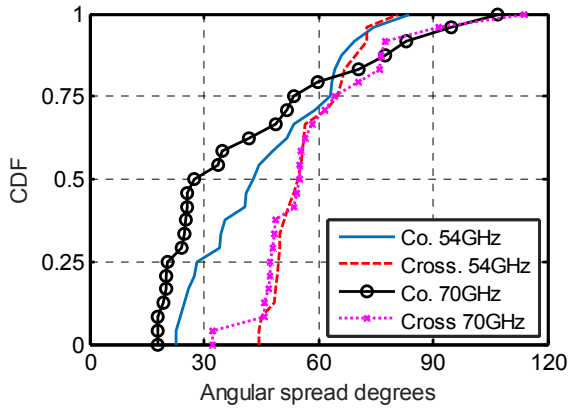

Fig. 6. *CDF of angular spread in the computer foyer*

For scenarios with low scatter density where the arriving signals are constrained along a particular direction such as in the corridor scenario low angular spread in the co-polar link can be observed. Across the measured scenarios, the difference of the average angular spread for both bands is less than 15°. Similar results were reported at 6-60 GHz [17] and 72 GHz [13].

Table 3 *Angular spread for the 54 GHz (70 GHz) band*

	Angular spread statistic in degrees CDF=50%; CDF=90%; $\sigma_{\emptyset_{rms}}$	
Scenario	Co-polar	Cross-polar
Factory	42.4; 52.5; 8 (41.2; 54.3; 12.6)	68.3; 77.2; 7.8 (68; 82.3; 12)
Corridor	28.3; 38.2; 6.9 (25.6; 37.3; 6.3)	71.3; 82.4; 13.5 (61.7; 77.9; 16.9)
Computer Foyer	43; 67.9; 17.9 (27.3; 80.8; 26.6)	(54.6; 71.5; 9.9) (55; 77.1; 17.6)
Office	40.5; 58.1; 11.9 (39.3; 57.4; 11.9)	74.1; 83; 10.2 (79.5; 97.2; 12.5)

3.2 Delay Spread

The channel *r.m.s.* delay spread (τ_{rms}) is often of interest in propagation studies as it provides a measure of the dispersive nature of the channel as a result of multipath. These multiple paths may constructively or destructively add to the desired signal therefore resulting in small-scale fading and inter-symbol interference [10] which are detrimental to system performance. The *r.m.s* delay spread, τ_{rms} given in (5), determines the maximum achievable data rate without the need for equalization [7].

$$\tau_{rms} = \sqrt{\frac{\sum_{n=1}^{N}(\tau_n-\tau_m)^2 P(\tau_n)}{\sum_{n=1}^{N} P(\tau_n)}} \quad (5)$$

where τ_n is the excess delay of the n^{th} delay bin, $P(\tau_n)$ the corresponding delay bin power, N is the number of delay bins in the profile and τ_m is the mean delay expressed as in (6).

$$\tau_m = \frac{\sum_{n=1}^{N} P(\tau_n)\tau_n}{\sum_{n=1}^{N} P(\tau_n)} \quad (6)$$

In each measurement position the *r.m.s.* delay spread was estimated for a 20-dB threshold from the peak in each individual PDP and categorised, depending on the relative angular orientation of the Tx and Rx antennas, as boresight (BS) when the antennas main beam are aligned and no obstruction in the link, or non-boresight (NBS) when the beams were not aligned or when there was an obstruction between the transmitter and receiver. PDPs with peak power to noise ratio less than 20 dB were excluded. Figure 7 shows the cumulative distribution function of the *r.m.s.* values for the factory scenario in both frequency bands. A summary of the *r.m.s.* delay spread, in *ns*, at 50% and 90% CDF levels and the corresponding standard deviation, for each scenario, are given in tables 4 and table 5 for boresight and non-boresight cases, respectively.

In all the scenarios, the non-boresight values are greater than the corresponding boresight values. This is due to either the absence of the direct component when the link is obstructed, or being weak, due to the misalignment of the antenna beams [18]. Similarly, cross-polar links exhibit larger *r.m.s.* delay spread compared to the co-polar links. Comparing the 50% CDF values of the two frequency bands, the 70 GHz band has a lower *r.m.s.* delay spread value than the 54 GHz band for the co-polar links in the boresight configuration.

A summary of the *r.m.s.* delay spread, in *ns*, at 50% and 90% CDF levels as well as the corresponding standard deviation ($\sigma_{\tau_{rms}}$), for each scenario, are given in tables 4 and 5.

Table 4 *Boresight delay spread at 54 GHz (70 GHz)*

	delay spread statistic CDF=50%; CDF=90%; $\sigma_{\tau_{rms}}$	
Scenario	Co-polar	Cross-polar
Factory	1.1; 3.1; 2.48 (0.8; 3.6; 2.7)	4.5; 16.1; 7.3 (4.3; 14.7; 7)
Corridor	0.7; 1.3; 0.4 (0.5; 1.2; 0.5)	5.2; 14.3; 6.9 (7.9; 21.5; 10.4)
Computer Foyer	1; 2.9; 1.2 (0.6; 2.4; 1.1)	2.3; 8.1; 3.8 (1.3; 5.4; 2.6)
Office	0.6; 0.8; 1.9 (0.4; 6.3; 4.7)	2.4; 12; 6.9 (6.6; 21.3; 9.9)

Table 5 *Non-boresight delay spread at 54 GHz (70 GHz)*

	delay spread statistic CDF=50%; CDF=90%; $\sigma_{\tau_{rms}}$	
Scenario	Co-polar	Cross-polar
Factory	14.7; 30.7; 11.2 (13.9; 30.4; 12.3)	15.8; 31.7; 11.5 (13.1; 27; 11.5)
Corridor	8.9; 44.6; 23.3 (6.1; 35.2; 18.6)	10.4; 43; 21.4 (6.4; 34.2; 17.6)
Computer Foyer	7.6; 29.7; 14.1 (10.9; 28.1; 13.6)	10.2; 31.9; 14.8 (8.6; 26.6; 12.6)
Office	7.6; 23.6; 10.7 (9.4; 25.5; 10.6)	10.2; 19.2; 6.8 (9.6; 19.2; 6.5)

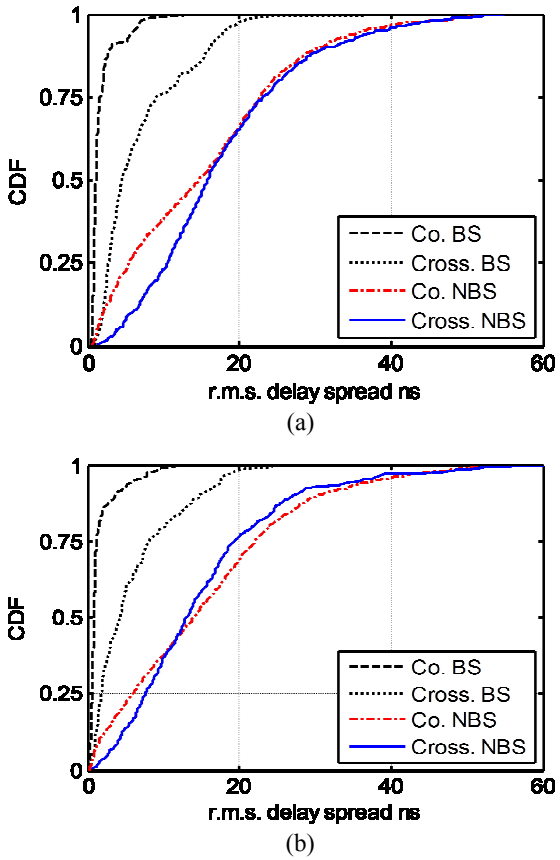

Fig. 7. *CDF of the r.m.s values for the factory scenario (a) 54 GHz and (b) 70 GHz*

3.3 Cross polarization ratio

The cross polarization ratio, (XPR), given in (6), is the ratio of the received power between co-polar and cross-polar links [19]. In each scenario the corresponding XPR value at individual angles, excluding those with no signal present, were combined into a single data pool for the computation of the CDF. Figure 8 shows the CDF of XPR values in the corridor scenario. Table 7 summarises the XPR values at 50% and 90% CDF level and the corresponding standard deviation (σ_{XPR}). The notation XPR_{HV} corresponds to the power ratio of the Tx-Rx co-polarised (H-H) link to that of the cross-polarised (H-V) link. Similarly, XPR_{VH} is the power ratio of the link V-V to that of V-H link.

$$XPR_{xy} = \frac{P_{Rxx}}{P_{Rxy}} \qquad (6)$$

where the subscript notation 'x' and 'y' relates to the antenna polarization, x ≠ y, and "P_R" is the corresponding received power.

The table indicates that across the scenarios and the frequency bands the average cross polarization discrimination ratio is less than ~ 18 dB.

Table 6 *XPR statistics for the 54 GHz (70 GHz) band*

	XPR values CDF=50%; CDF=90%; σ_{XPR}	
Scenario	XPR_{HV}	XPR_{VH}
Factory	11.7; 17.1; 4 (7.5; 15.2; 5.40)	12.4; 17.1; 3.5 (15.7; 20.3; 3.3)
Corridor	13.1; 24.9; 7.4 (7.7; 21.9; 8.4)	13.9; 21.7; 5 (16.5; 25.4; 6.2)
Computer Foyer	14.2; 22.6; 4.9 (11.6; 21.6; 6)	14.4; 21.6; 4.4 (17.6; 25.5; 5.1)
Office	13.2; 25.5; 7.3 (7.9; 22; 8.5)	13.8; 20.3; 4.6 (16.4; 23.9; 5.2)

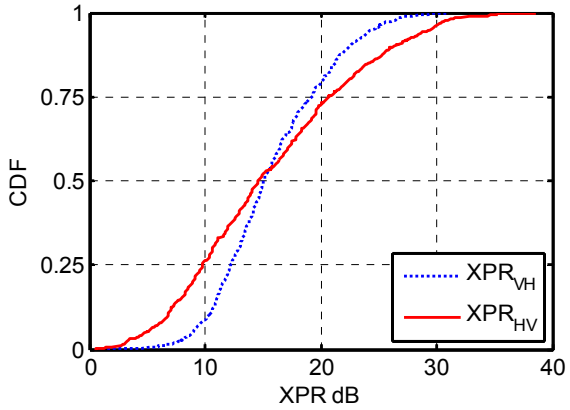

Fig. 8 *XPR values for the 54 GHz band in the corridor scenario*

3.4 Path Loss

Path loss provides an estimation of the signal attenuation as it propagates through the environment, and it is an important element in the design of the link

budget of wireless communication systems. Path loss describes the ratio of transmitted power to that of the received power excluding the overall system gain and the gains of the antennas. For the estimation of path loss, the received power of a synthesised omnidirectional antenna for each location is estimated from the directional measurements by summing the received power from all angles [20, 21], excluding those with only noise. Since in the present measurements, the angle of rotation was smaller than the 3-dB beamwidth, the additional gain due to the overlap of the antenna pattern had to be accounted for in the estimation of the path loss. This was estimated by synthesising the omni-directional power from the measured response in an anechoic environment and subtracting the additional antenna gain resulting from the overlap of the beams as outlined in [22].

The parameters of the single frequency path loss models, including *log-distance model and close-in model* were estimated. For the log-distance path loss model, given in (7), two parameters are needed: the path loss intercept at a metre distance "PL_o", in dB, and the dimensionless path loss coefficient "α". For the close-in free space model, given in (8), only the dimensionless path loss coefficient parameter "n" needs to be estimated as the path loss intercept is assumed that of free space loss at 1 m. The parameter "f_o", in (8) in MHz, is the operating central frequency.

$$PL_{logDist}(d) = PL_o + 10\alpha \log_{10}(d) \quad (7)$$

$$PL_{CI}(d) = 20\log_{10}(f_o) - 27.55 + 10n \log_{10}(d) \quad (8)$$

In the above models, "d" refers to the 3D distance between the transmitting and receiving antennas. The models parameters were estimated through the least squares regression method, as in [10]. The method finds the optimum value of the corresponding parameters that minimize the standard deviation (σ, in dB) of the error between the computed and measured path loss.

Figure 9 displays the measured path loss data and the corresponding model fit for the co-polar and cross-polar measurements as well as the theoretical free space path loss in both frequency bands in the computer foyer scenario.

Tables 7 and 8 summarise the values of the estimated path loss parameters for the close-in model and log-distance model respectively. For the clos-in model only the co-polarised links are displayed in the figures and given in Table 7 as this model gave significantly higher standard deviation e.g. 5.3 versus 2.3 for the corridor scenario. Table 8 indicates that across the scenarios the path loss intercept point (PL_o) of the cross-polarised link is higher than that of its co-polarised counterpart. This additional loss is due to the polarisation mismatch. Moreover, the results show that the log-distance path loss model provides a better fit, i.e. smaller standard deviation, in comparison with the close-in model. Across the scenarios and frequency bands the path loss exponents vary in the range of 1.5-2 (co-polar), for the close-in model, and 0.9-1.9 (co-polar) and 1-1.8 (cross-polar) for the log-distance model.

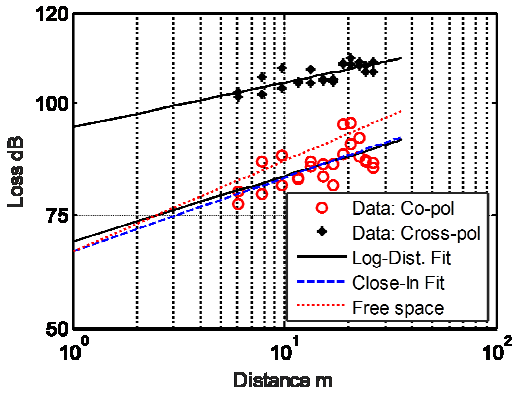

(a)

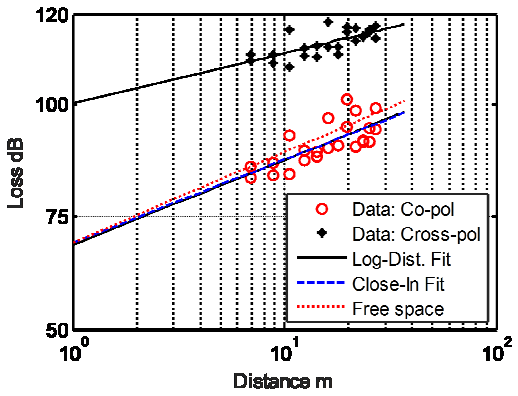

(b)

Fig. 9 *Path loss in the computer foyer scenario at (a) 54 GHz and (b) 70 GHz*

Table 7 *Close-in model for the 54 GHz (70 GHz) band*

	Parameter values $n; \sigma$	
Scenario	Co-polar	Cross-polar
Factory	1.8; 1.1 (1.8; 2.4)	- -
Corridor	1.5; 1.7 (1.5; 2.3)	- -
Computer foyer	1.7; 3.4 (1.8; 3.1)	- -
Office	2; 1.6 (1.9; 2.2)	- -

Table 8 *Log-distance model for the 54 GHz (70 GHz) band*

	Log-Distance model parameter α; PL_o; σ	
Scenario	Co-polar	Cross-polar
Factory	1.4; 71.3; 0.8 (0.9; 80.1; 1.5)	1.5; 87.5; 1 (1.1; 94.9; 1.9)
Corridor	1.5; 65.9; 1.6 (1.2; 72.9; 2.2)	1.7; 86.5; 2.8 (1.8; 88.7; 4.1)
Computer foyer	1.5; 69.2; 3.3 (1.9; 68.7; 3.1)	1; 94.6; 1.5 (1.1; 100.1; 2)
Office	1.7; 70.1; 1.5 (1.7; 71.8; 2.2)	1.8; 90.9; 2.4 (1.5; 96.3; 1.7)

4. Conclusions

A wideband MIMO FMCW channel sounder was used to study millimetre-wave channel propagation in various indoor scenarios. Dual polarized measurements were performed in the frequency bands centred at 54 GHz and 70 GHz to investigate the temporal and angular small-scale statistics of the indoor radio channel. Additionally, parameters of the single and multi-frequency path loss models were estimated from the data. It was observed that for co-polarized links, in LOS conditions, the average delay spread increases when the Rx antenna beam is not aligned with the Tx antenna beam. Moreover, the 54 GHz band produced higher average *r.m.s* delay spread than the 70 GHz. Azimuthal receiver angular spread in the co-polar links is smaller than the cross-polar counterpart. The results also show no obvious frequency dependence characteristics of the azimuthal angular spread.

5. Acknowledgement

The 60 GHz sounder was developed under the EPSRC grant PATRICIAN EP/I00923X/1. The upgrade to the WRC15 frequency bands and the measurements reported in the paper are funded under an Ofcom contract Number 1362 on 'Long term measurements campaign and development of model(s) for mm wave bands (30-90 GHz)', and EPSRC impact acceleration account, IAA. The upgrade of the sounder to the WRC15 frequency bands was realised by the late Stuart Feeney.

6. References

[1] Rangan, S., Rappaport, T., Erkip, E., "Millimeter-wave cellular wireless networks: potentials and challenges," IEEE Proc., 2014, 102, (3), pp. 366-385.

[2] Karjalainen, J., Nekovee, M., Benn, H., et al., "Challenges and opportunities of mm-wave communication in 5G networks," 9th Int. Conf. on Cognitive Radio Oriented Wireless Networks and Communications (CROWNCOM), Oulu, Finland, June 2014, pp. 372-376.

[3] Piersanti, S., Annoni, L., Cassioli, D., "Millimeter waves channel measurements and path loss models," IEEE Int. Conf. on Communications (ICC), Ottawa, Canada, June 2012, pp. 4552-4556.

[4] Salous, S., Feeney, S., Raimundo, X., et al., "Wideband MIMO channel sounder for radio measurements in the 60 GHz band," IEEE Transactions on Wireless Communications, 2016, 15, (4), pp. 2825-2832.

[5] Karadimas, P., Allen, B., Smith, P. "Human body shadowing characterization for 60-GHz indoor short-range wireless links". IEEE Antennas and Wireless Propagation Letters, 2013, 12, pp. 1650-1653.

[6] Guerra, A., Guidi, F., Clemente, A., et al., "Delay spread characterization of millimeter-wave indoor backscattering channel," 10th European Conf. on Antennas and Propagation (EuCAP), Davos, Switzerland, April 2016, pp. 1-2.

[7] Hao Xu, Kukshya, V., Rappaport, T., "Spatial and temporal characteristics of 60-GHz indoor channels," IEEE Journal on Selected Areas in Communications, 2002, 20, (3), pp. 620-630.

[8]Wu, X., Wang, C., Sun, J., et al., "60-GHz millimeter-wave channel measurements and modeling for indoor office environments," IEEE Transactions on Antennas and Propagation, 2017, 65, (4), pp. 1912-1924.

[9] Anderson, C., Rappaport, T., Bae, K., et al., "In-building wideband multipath characteristics at 2.5 and 60 GHz," Proc. IEEE 56th Vehicular Tech. Conf. September 2002, Vancouver, pp. 97-101.

[10] Maccartney, G., Rappaport, T., Sun, S., et al., "Indoor office wideband millimeter-wave propagation measurements and channel models at 28 and 73 GHz for ultra-dense 5G wireless networks," IEEE Access, 2015,3, pp. 2388-2424,.

[11] J. Zhu, H. Wang and W. Hong, "Large-scale fading characteristics of indoor channel at 45-GHz band," IEEE Antennas and Wireless Propagation Letters, 2015, 14, pp. 735-738.

[12] Haneda, K., Järveläinen, J., Karttunen, A., et al., "Indoor short-range radio propagation measurements at 60 and 70 GHz," The 8th European Conf. on Antennas

and Propagation (EuCAP 2014), The Hague, Netherlands, April 2014, pp. 634-638.

[13] Bamba, A., Mani, F., D'Errico, R., "E-band millimeter wave indoor channel characterization," IEEE 27th Annual Int. Symposium on Personal Indoor and Mobile Radio Communications (PIMRC), Valencia, Spain, September 2016, pp. 1-6.

[14] Wang, Q., Li, S., Zhao, X., et al., "Wideband millimeter-wave channel characterization based on los measurements in an open office at 26 GHz," IEEE 83rd Vehicular Technology Conf. (VTC Spring), Nanjing, China, May 2016, pp.1-5.

[15] Fleury, B., "First- and second-order characterization of direction dispersion and space selectivity in the radio channel," IEEE Transactions on Information Theory, 2000, 46, (6), pp. 2027-2044.

[16] Zhang, N., Yin, X., Lu, S., Du, M., Cai, X., "Measurement-based angular characterization for 72 GHz propagation channels in indoor environments, " 2014 IEEE Globecom Workshops (GC Wkshps), Texas, USA, December 2014, pp. 370-376.

[17] Medbo, J., Seifi, N., Asplund, H., "Frequency Dependency of Measured Highly Resolved Directional Propagation Channel Characteristics," 22th European Wireless Conf., Oulu, Finland, May 2016, pp. 1-6.

[18] R., Weiler, M., Peter, T., Kühne, at el., "Simultaneous millimeter-wave multi-band channel sounding in an urban access scenario," 9th European Conf. on Antennas and Propagation (EuCAP), Lisbon, Portugal, August 2015, pp. 1-5.

[19] Gurrieri, L., Noghanian, S., Willink, T.,"Indoor wireless reception improvement using cross-polarized multipath signals," 12th Int. Symposium on Antenna Technology and Applied Electromagnetics and Canadian Radio Sciences Conf., Montreal, Canada, July 2006, pp. 1-4.

[20] Sun, S., MacCartney, G., Samimi, M., et al.,"Synthesizing omnidirectional antenna patterns, received power and path loss from directional antennas for 5G millimeter-wave communications," IEEE Global Communications Conf. (Globecom), San Diego, USA, December 2015, pp.1-6.

[21] Deng, S., Samimi, M., Rappaport, T., "28 GHz and 73 GHz millimeter-wave indoor propagation measurements and path loss models," IEEE International Conf. on Communication Workshop (ICCW), London, United Kingdom, June 2015, pp. 1244-1250.

[22] Salous, S., Raimundo, X., Cheema, A., "Path loss model in typical outdoor environments in the 50–73 GHz band," 11th European Conf. on Antennas and Propagation (EUCAP), Paris, France, March 2017, pp. 721-724.